Simple and Seamless PWM Scheme of Isolated Bidirectional AC–DC Converter for Reducing Voltage Spike

Jeong-Tae Kim, *Student Member, IEEE*, and Sung-Min Park, *Member, IEEE*

***Abstract*—This article proposes an improved modulation scheme based on unipolar sinusoidal pulsewidth modulation for a single-phase single-stage isolated bidirectional ac–dc converter. A direct ac–ac conversion system connected with a high-frequency transformer typically suffers from high-voltage spikes because of the leakage inductors of the high-frequency transformer and the grid filter inductors, resulting in reduced reliability and large power losses. The proposed modulation scheme can eliminate the high-voltage spikes in bidirectional power flow without the use of additional circuits while realizing zero-voltage switching. In addition, because the proposed method does not require individual gate control of the bidirectional power switches, the generation of gate signals can be simplified using the proposed modulation scheme. A simulation model and a 1.2 kW grid-connected ac–dc converter based on silicon-carbide metal–oxide–semiconductor field-effect transistors are implemented to validate the effectiveness of the proposed modulation scheme.**

***Index Terms*—Cycloconverter-type high-frequency link converter, isolated bidirectional ac–dc converter, matrix-type converter, modulation scheme, zero-voltage switching (ZVS).**

I. Introduction

GALVANICALLY isolated power converters have been used in various applications, such as uninterruptible power supply, electric vehicle battery chargers, and renewable power generation systems, to physically and electrically separate the input and output ports [1]–[6]. Typically, high-frequency transformers (HFTs) that can operate at high switching frequencies have been employed in specific power conversion systems requiring isolation capability owing to their reduced size and these power conversion systems are called high-frequency link (HFL) based converters.

Generally, HFL-based converters can be classified into the dual active bridge (DAB) and cycloconverter-type converters. DAB-type converters are more prominently used in commercial and industrial applications than the latter owing to the easy realization from their intuitive circuit structure and simple control scheme. However, multistage circuit structures with bulky electrolytic capacitors may hinder the improvement in the power density and reliability of systems [7], [8]. In contrast, in the case of cycloconverter-type HFL (CHFL) converters, the electrolytic capacitors can be removed owing to the direct ac–ac conversion configuration using bidirectional power switches with a single-stage circuit structure, resulting in improved power density and reliability of the system.

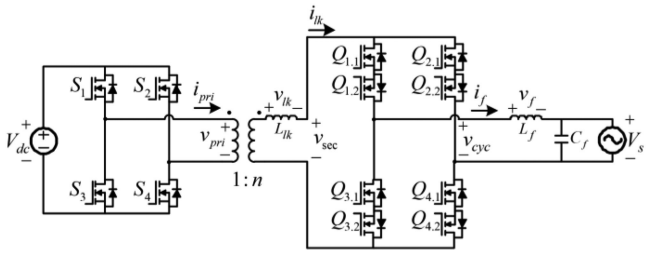

Fig. 1. Circuit configuration of CHFL converter.

Fig. 1 depicts the circuit configuration of a CHFL converter consisting of a full-bridge (FB) converter, a cycloconverter, and an HFT. The FB converter is connected to a dc link for dc–ac conversion, whereas the cycloconverter employing bidirectional switches is connected to the grid for ac–ac conversion. It can be seen that both converters are linked by an HFT. The undesirable conditions under this structure are that both the HFT leakage inductor and filter inductor act as current sources and possess a series connection during intermediate switching states. These conditions cause the HFT leakage current to abruptly rise during ac–ac conversion, leading to high-voltage-spike problems across power devices. Consequently, this problem deteriorates the efficiency and reliability of the CHFL converter system.

To resolve the above problems related to the high-voltage spikes, several solutions have been studied [9]–[20], which are categorized based on the requirement of additional circuits on the HFT side of the cycloconverter. Adding resistor–capacitor and resistor–capacitor–diode snubber circuits is a simple solution; however, the system efficiency decreases because of the resistor heat dissipation [9], [10]. In contrast, although clamp circuits have no resistor heat dissipation, they may increase the system complexity and cost owing to the requirement of additional

Manuscript received October 8, 2021; revised January 11, 2022; accepted February 18, 2022. Date of publication March 3, 2022; date of current version April 28, 2022. This work was supported by the National Research Foundation of Korea Grant funded by the Korea Government (MSIT) under Grants 2017R1C1B2008200 and 2020R1F1A1071598. Recommended for publication by Associate Editor D. Vinnikov. *(Corresponding author: Sung-Min Park.)*

The authors are with the Department of Electronic and Electrical Engineering, Hongik University, Sejong 30016, South Korea (e-mail: wjdxo0220@naver.com; smpark@hongik.ac.kr).

Color versions of one or more figures in this article are available at https://doi.org/10.1109/TPEL.2022.3155824.

Digital Object Identifier 10.1109/TPEL.2022.3155824

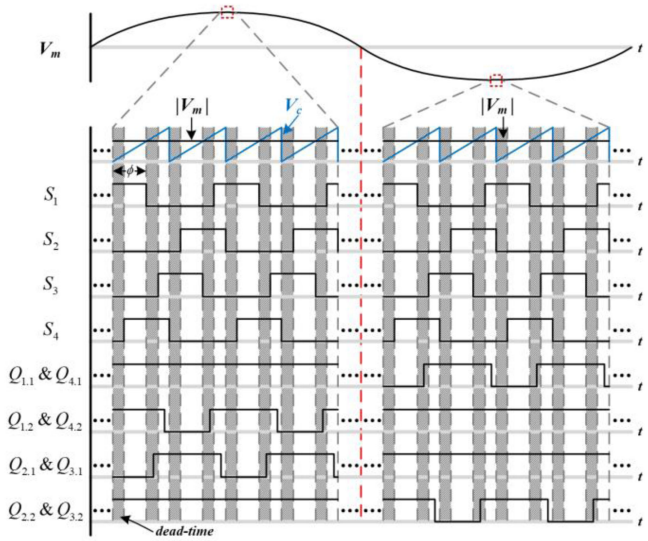

Fig. 2. Switching-signal waveform of the proposed modulation scheme.

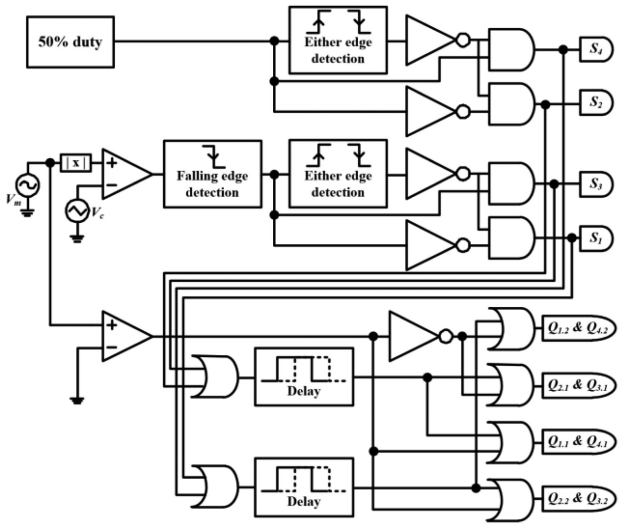

Fig. 3. Function block diagram of the proposed modulation scheme.

components, such as transformers, diodes, and power switches [11]–[13].

Several modulation schemes that do not require additional circuits have been studied to deal with the above-mentioned high-voltage-spike problems [14]–[20]. However, their effectiveness is highly dependent on the power flow direction (dc-to-ac or ac-to-dc). The modulation schemes in [14]–[18] allow the HFT leakage-inductor current to reach the filter inductor current smoothly via natural rectification, thereby eliminating the high-voltage spikes effectively in the discharging mode (dc-to-ac conversion). However, this method cannot be applied to the charging mode (ac-to-dc conversion) because the rising direction of the HFT leakage-inductor current is different from the discharging mode. A modulation scheme for the charging mode was proposed in [19], wherein the HFT leakage-inductor was charged in advance by applying a short-time reverse voltage. However, in the discharging mode, it is inherently impossible to

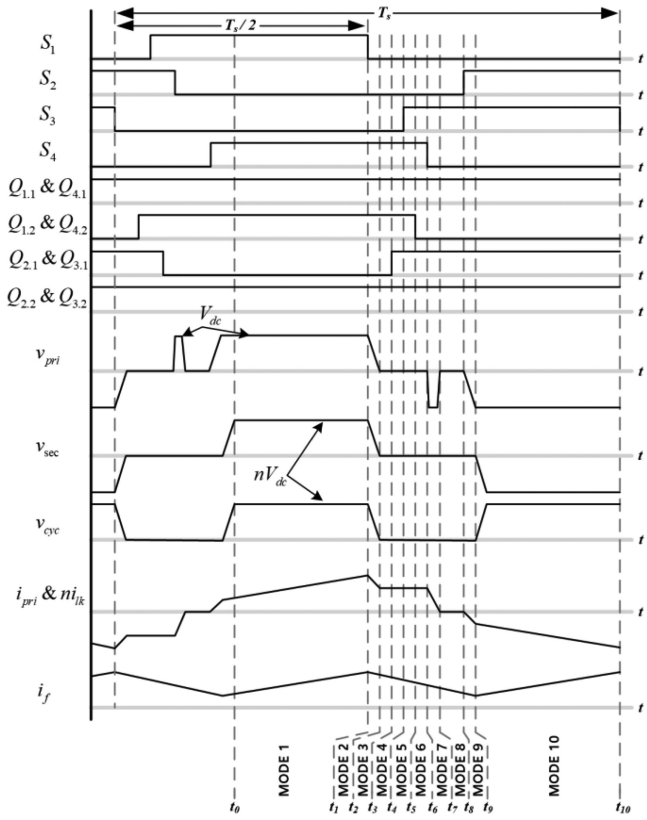

Fig. 4. Principal operating waveforms and gate signals in discharging mode.

control the output power owing to the reverse current blocking function of the free-wheeling diodes on the cycloconverter side. Recently, with the unified effective method becoming available in both discharging and charging modes, a hybrid-type modulation scheme combining two different modulation schemes was proposed in [20]. In this scheme, the HFT leakage-inductor current increases smoothly in the discharging mode and the HFT leakage-inductor is precharged in the charging mode. However, it may be difficult to determine the operation mode correctly between discharging and charging because two independent modulation schemes are employed simultaneously based on the power conversion direction, resulting in an unsatisfactory performance under certain power control scenarios, such as reactive power compensation. In addition, the modulation scheme is complex because all the power switches on the cycloconverter side need to be individually controlled.

This article proposes an improved modulation scheme for an ac–ac conversion structure using bidirectional switching devices. By controlling two pairs of ac ON-state switches used to form a natural commutation path (NCP), forming a continuous closed connection between the HFT and the grid, the HFT leakage-inductor current can increase smoothly in the discharging mode. In addition, two other pairs of ac switches are controlled based on the deadtime used in the H-bridge leg of the FB converter to discharge and precharge the HFT leakage inductor. Therefore, a transient voltage ***di/dt*** on the HFT leakage inductor can be reduced in the charging mode. Using the proposed method, elimination of high-voltage spikes and realization

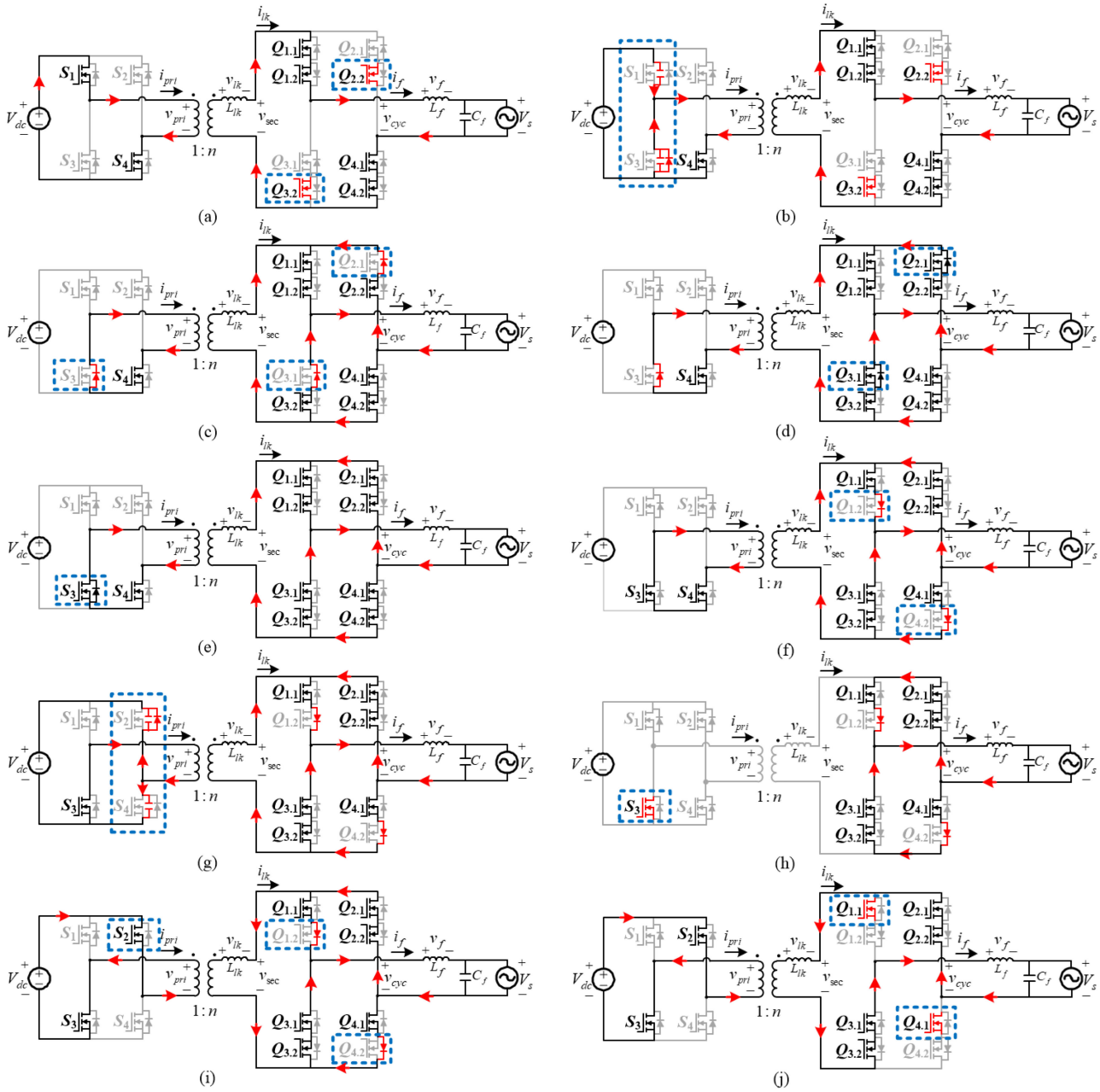

Fig. 5. Schematic of different operating modes using the proposed modulation in discharging mode. (a) MODE 1. (b) MODE 2. (c) MODE 3. (d) MODE 4. (e) MODE 5. (f) MODE 6. (g) MODE 7. (h) MODE 8. (i) MODE 9. (j) MODE 10.

of zero-voltage switching (ZVS) can be achieved simultaneously in all operation modes; thus, the reliability and efficiency of the CHFL converter can be improved. In addition, the proposed method achieves a simpler switching-signal generation using only four gate signals for four pairs of ac switches compared that in [20] in which eight switching signals are used for the same purpose by determining the power reverse zone.

The rest of this article is organized as follows. Section II presents the proposed modulation scheme as well as the detailed analysis of its operating principles in both discharging and charging modes. The simulation and the experiment are described in Section III and Section IV, respectively. Finally, Section V concludes this article.

II. Principle of the Proposed Modulation Technique

Fig. 2 shows the switching-signal waveforms of the proposed method, where V_m and V_c are the modulation voltage and the carrier voltage, respectively. The FB converter uses a unipolar phase-shifted modulation scheme to control the power flow and realize ZVS. Switches S_1, S_2, S_3, and S_4 have a 50% duty cycle, and the phase angle (ϕ) can be determined by comparing the absolute values of V_m and V_c. The cycloconverter uses a unipolar sinusoidal pulsewidth modulation (SPWM) based modulation scheme. The gate signals of four pairs of ac switches are determined by V_m and the switching signals of the FB converter. To operate the CHFL converter in the discharging

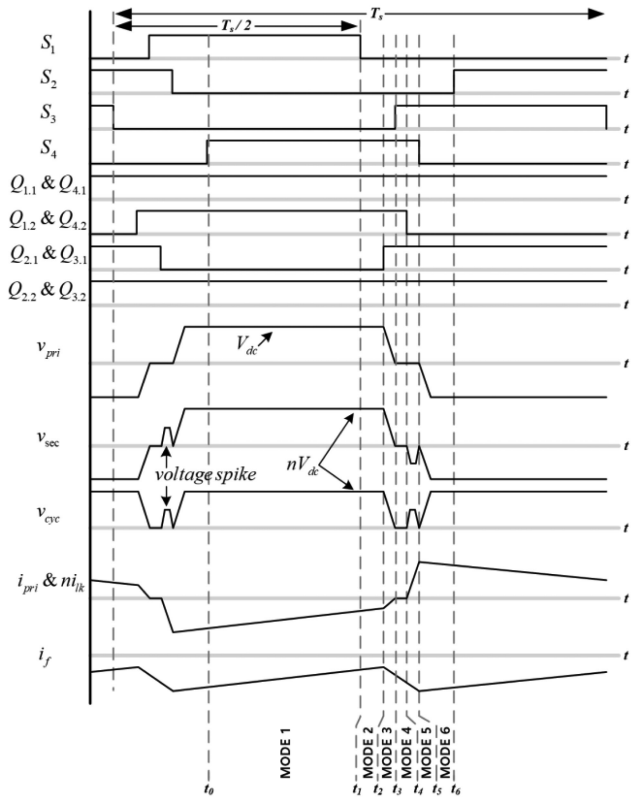

Fig. 6. Principal operating waveforms and gate signals in charging mode.

mode, ac switches $Q_{1.1}$, $Q_{2.2}$, $Q_{3.2}$, and $Q_{4.1}$ are always in the ON-state when V_m is positive. In contrast, when V_m is negative, the ac switches are switched in the opposite scheme. These ac switching principles allow the HFT leakage-inductor current to reach the filter inductor current smoothly by forming an NCP. Therefore, the high-voltage spikes can be removed in the discharging mode. For the operation of the CHFL converter in the charging mode, the ac switches under the NCP conditions are switched on the basis of the deadtime of the FB converter. First, the ac switches are turned ON during the deadtime period to discharge the HFT leakage-inductor energy back to the dc link before starting the free-wheeling path of the FB converter. Second, the ac switches are turned OFF before the deadtime to precharge the HFT leakage inductor using the filter inductor current before the HFT is applied with the dc-link voltage. Based on these ac switching principles producing a transient voltage at zero voltage, the transient voltage, ***di/dt***, can be reduced in the charging mode. Fig. 3 shows the function block diagram of the proposed modulation scheme. Using this block embedded in the microcontroller, the firing pulsewidth modulation signals can be generated properly for the proposed modulation scheme.

A. Description and Analysis of the Proposed Modulation Scheme in Discharging Mode

In this section, the proposed modulation scheme in the discharging mode and its analysis are described in detail on the basis of key waveforms and schematics. Fig. 4 shows the principal operating waveforms and the gate signals in different switching states. In addition, Fig. 5 displays the corresponding schematics depicting the conduction paths and switching states. The operating modes are described as follows.

MODE 1 [t_0–t_1, Fig. 5(a)]: Switches S_1, S_4, $Q_{1.1}$, $Q_{1.2}$, $Q_{2.2}$, $Q_{3.2}$, $Q_{4.1}$, and $Q_{4.2}$ are in the ON-state in which the current does not flow through $Q_{2.2}$ and $Q_{3.2}$. By charging the filter inductor, the filter inductor current (i_f) increases with the incremental change, which can be represented as

$$\Delta i_f = \Delta i_{\rm lk} = \frac{nV_{\rm dc} - V_s}{L_f + L_{\rm lk}}(t_1 - t_0). \tag{1}$$

where $i_{\rm lk}$, $V_{\rm dc}$, V_s, L_f, $L_{\rm lk}$, and n are the HFT leakage-inductor current, dc-link voltage, grid voltage, filter inductance, HFT leakage inductance, and transformer turns ratio, respectively. It can be noted that the HFT leakage-inductor current becomes the filter inductor current with a positive value and the current does not flow through the body diodes of $Q_{1.2}$ and $Q_{4.2}$.

MODE 2 [t_1–t_2, Fig. 5(b)]: At the beginning of this interval, switch S_1 is turned OFF. The output capacitor of S_1 starts to be charged, whereas that of S_3 is discharged. The primary-side current $i_{\rm pri}$ begins to flow through the body diode of S_3. Both primary-side voltage $v_{\rm pri}$ and secondary-side voltage $v_{\rm sec}$ decrease from positive to zero. The primary-side voltage can be expressed as

$$v_{\rm pri}(t) = \frac{1}{n}v_{\rm sec}(t) = V_{\rm dc} - \frac{1}{C_{OSS}}\int_{t_1}^{t} i_{\rm pri}(t)dt. \tag{2}$$

where C_{OSS} is the output capacitance of the power switch used in the CHFL converter. By discharging $L_{\rm lk}$, the instantaneous value representing the magnitude of the HFT leakage-inductor current at point t_2 can be written as

$$i_{\rm lk}(t_2) = i_{\rm lk}(t_1) - \frac{1}{L_{\rm lk}}nV_{\rm dc}(t_2 - t_1). \tag{3}$$

MODE 3 [t_2–t_3, Fig. 5(c)]: Power switches S_1 and S_3 in the FB converter are in the OFF-state, and the deadtime begins when the transformer primary currents start to free wheel through the body diode of S_3. Because the forward voltage of a body diode is considerably smaller compared with the dc-link voltage, it can be assumed that $v_{\rm pri}$ and $v_{\rm sec}$ become zero. Thus, currents $i_{\rm pri}$ and $i_{\rm lk}$ ideally become constant until upcoming MODE 6 when the free-wheeling path ends. On the cycloconverter side, i_f flows through the body diodes of $Q_{2.1}$ and $Q_{3.1}$, and the stored energy in the filter inductor is discharged, resulting in decreased filter inductor current. The incremental change in the filter inductor current can be expressed as

$$\Delta i_f = \frac{v_f}{L_f}(t_9 - t_2) \approx \frac{-V_s}{L_f}(t_9 - t_2). \tag{4}$$

where v_f is the filter inductor voltage. It can be noted that v_f in (4) can be replaced by $-V_s$ because the HFT leakage-inductor voltage ($v_{\rm lk}$) is zero.

MODE 4 [t_3–t_4, Fig. 5(d)]: This mode is initiated during the deadtimes of S_1 and S_3 to prevent the short circuit of the cycloconverter. It can be seen that the ZVS operation can be

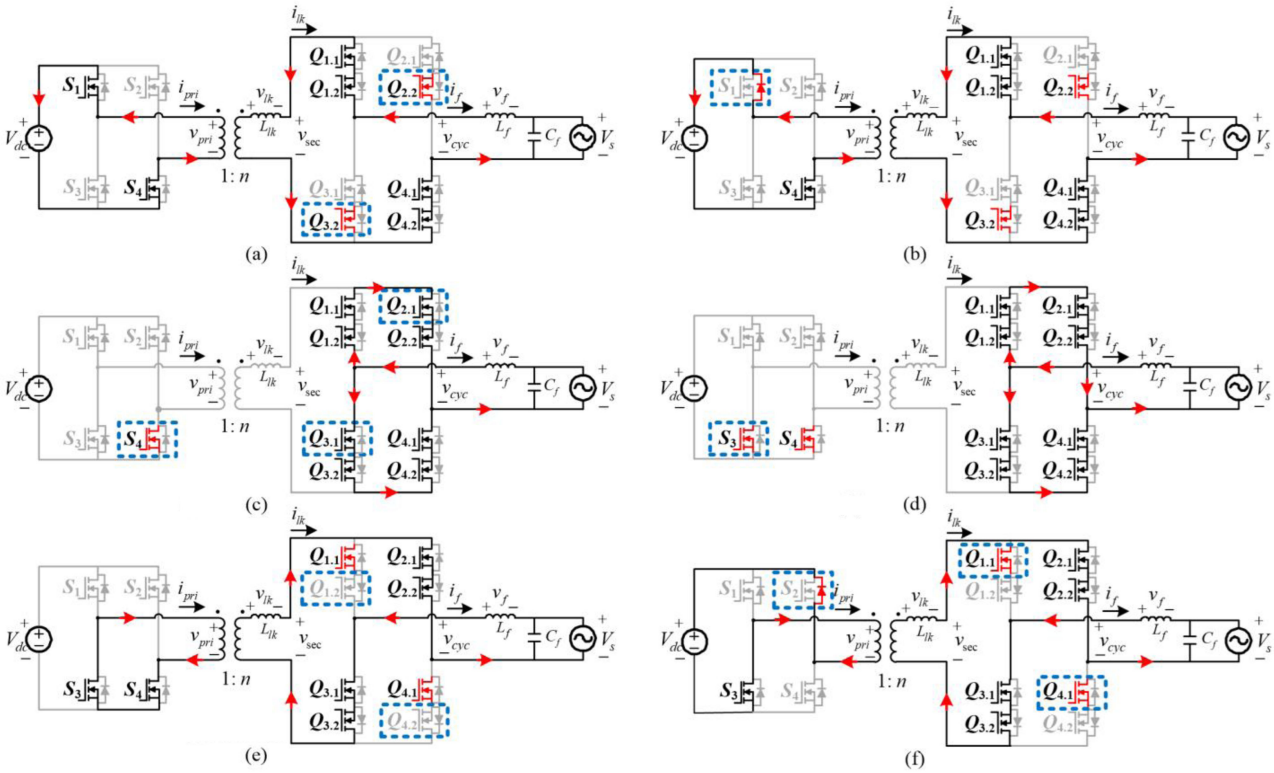

Fig. 7. Schematic of different operating modes using the proposed modulation in charging mode. (a) MODE 1. (b) MODE 2. (c) MODE 3. (d) MODE 4. (e) MODE 5. (f) MODE 6.

achieved by turning ON switches $Q_{2.1}$ and $Q_{3.1}$ because input voltage $v_{\rm sec}$ from the cycloconverter is zero.

MODE 5 [t_4–t_5, Fig. 5(e)]: At the end of the deadtime, switch S_3 is turned ON under the ZVS operation because $i_{\rm pri}$ flows through the body diode.

MODE 6 [t_5–t_6, Fig. 5(f)]: When this mode begins, ac switches $Q_{1.2}$ and $Q_{4.2}$ are turned OFF under ZVS because $v_{\rm sec}$ is zero and i_f flows through the body diodes of $Q_{1.2}$ and $Q_{4.2}$.

MODE 7 [t_6–t_7, Fig. 5(g)]: In this mode, switch S_4 is turned OFF. The output capacitor of S_4 is charged, whereas that of S_2 is discharged. During this mode, $|i_{\rm pri}| > 0$ and $i_{\rm pri}$ flows through the body diode of S_2. Therefore, $v_{\rm pri} = -V_{\rm dc}$, and the stored energy in the HFT leakage inductor $L_{\rm lk}$ starts to be discharged. The incremental change in the HFT leakage-inductor current $\Delta i_{\rm lk}$ can be expressed as

$$\Delta i_{\rm lk} = \frac{-nV_{\rm dc}}{L_{\rm lk}}(t_7 - t_6). \tag{5}$$

when $|i_{\rm pri}|$ becomes zero, this mode ends and the output capacitor of S_2 is charged again to $V_{\rm dc}$.

MODE 8 [t_7–t_8, Fig. 5(h)]: This mode is initiated during the deadtimes of S_2 and S_4; in this mode, the stored energy in the HFT leakage inductor $L_{\rm lk}$ is completely discharged and $i_{\rm pri}$ and $i_{\rm lk}$ approach zero at t_7. HFT voltages $v_{\rm pri}$ and $v_{\rm sec}$ become zero because the output capacitor of S_2 is recharged to $V_{\rm dc}$. It can be seen that only S_3 in the FB converter is in the ON-state, and the current flows through the cycloconverter.

MODE 9 [t_8–t_9, Fig. 5(i)]: In this mode, switch S_2 is turned ON. The primary-side voltage starts to decrease from zero to negative. The output voltage in the FB converter $v_{\rm pri}$ can be expressed as

$$v_{\rm pri}(t) = 0 - \frac{1}{C_{OSS}}\int_{t_8}^{t} i_{\rm pri}(t)dt. \tag{6}$$

The HFT leakage inductor $L_{\rm lk}$ is charged, and $i_{\rm lk}$ starts to decrease from zero to negative. The filter inductor L_f is discharged because i_f flows through the body diodes of $Q_{1.2}$ and $Q_{4.2}$. It should be noted that this mode continues until $|i_{\rm lk}|$ and i_f are equal.

MODE 10 [t_9–t_{10}, Fig. 5(j)]: In this mode, from the cycloconverter side, $|i_{\rm lk}|$ and i_f are equal. The filter inductor current does not flow through the body diodes of $Q_{1.2}$ and $Q_{4.2}$. The secondary-side voltage reaches $-nV_{\rm dc}$, and L_f is charged. The incremental change in the filter inductor current can be represented as

$$\Delta i_f = |\Delta i_{\rm lk}| = \frac{nV_{\rm dc} - V_s}{L_f + L_{\rm lk}}(t_{10} - t_9). \tag{7}$$

It can be seen that the current does not flow through $Q_{1.1}$ and $Q_{4.1}$. MODE 10 ends when S_3 is turned OFF. This interval returns to MODE 2; however, the voltage and current of the HFT are in the opposite direction of the direction in the previous switching cycle.

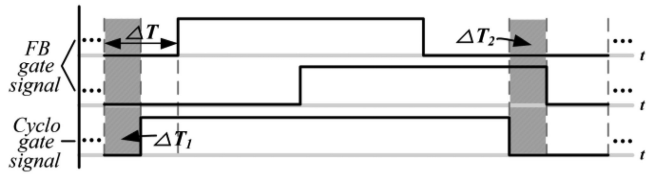

Fig. 8. Gate signals from the proposed modulation scheme.

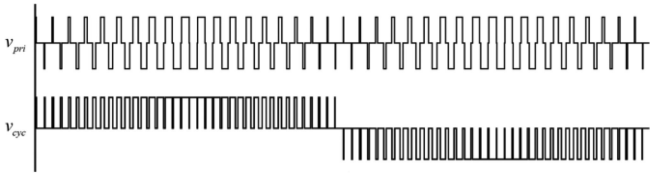

Fig. 9. Power conversion process of the CHFL converter.

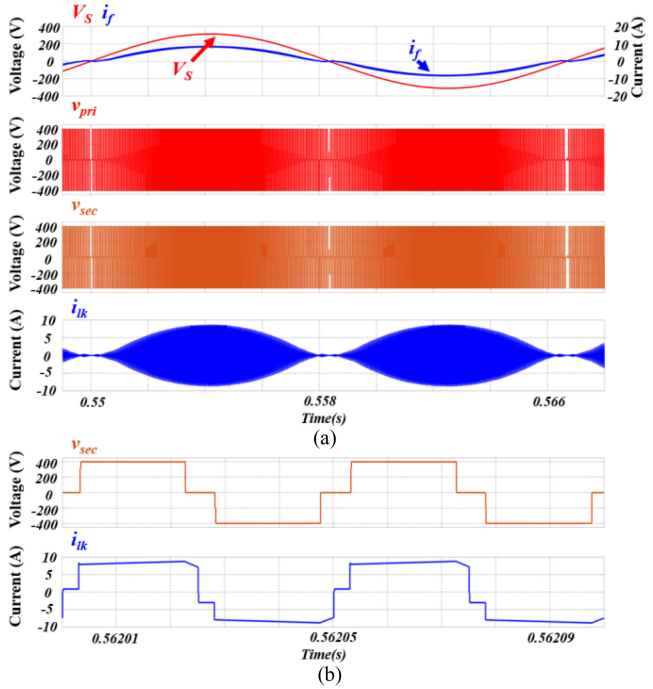

Fig. 10. Simulation results. (a) Voltages and currents in discharging mode. (b) Magnified simulation waveforms in discharging mode.

B. Description and Analysis of the Proposed Modulation Scheme in Charging Mode

The operation of the proposed modulation scheme in charging mode and its analysis are presented in detail using key waveforms and schematics. Fig. 6 shows the principal operating waveforms and gate signals in different operating modes. Additionally, Fig. 7 depicts the corresponding schematics.

MODE 1 [t_0–t_1, Fig. 7(a)]: In this mode, the switch operation is the same as that in MODE 1 in the discharging mode. However, $i_{\rm lk}$ and i_f are negative (not positive). The filter inductor is discharged, and $\Delta|i_f|$ can be expressed as

$$\Delta\,|i_f| = \frac{-nV_{\rm dc} + V_s}{L_f + L_{\rm lk}}(t_1 - t_0). \tag{8}$$

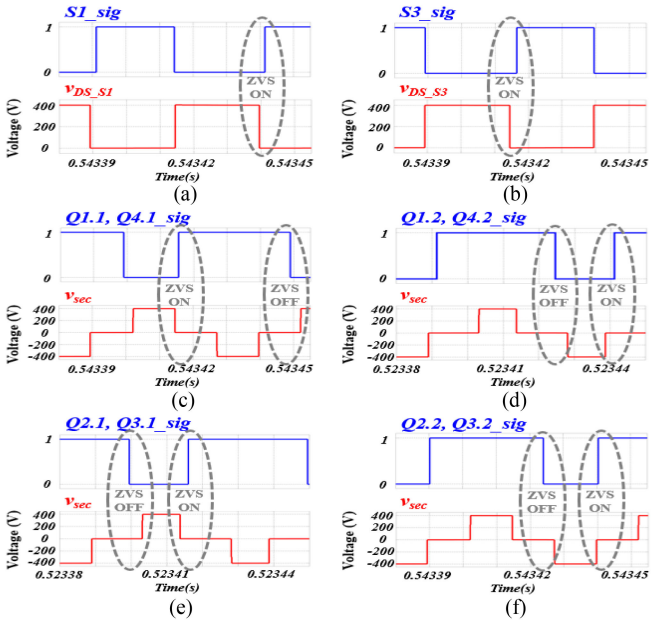

Fig. 11. Simulation results of the proposed modulation in discharging mode. (a) and (b) Gate signals and drain–source voltages of FB converter. (c)–(f) Gate signals and input voltage of cycloconverter.

The currents do not flow through switches $Q_{2.2}$ and $Q_{3.2}$ and the body diodes of $Q_{1.1}$ and $Q_{4.1}$.

MODE 2 [t_1–t_2, Fig. 7(b)]: In this mode, switch S_1 in the FB converter is turned OFF under ZVS because $i_{\rm pri}$ flows through the body diode. Both $L_{\rm lk}$ and L_f are discharged through the same current paths as in MODE 1.

MODE 3 [t_2–t_3, Fig. 7(c)]: In this mode, switches $Q_{2.1}$ and $Q_{3.1}$ are turned ON. All switches in the CHFL converter are in the ON-state and i_f free wheels through the ac switches. By charging L_f, the magnitude of the filter inductor current ($|i_f|$) increases incrementally, which can be expressed as

$$\Delta\,|i_f| = \frac{-v_f}{L_f}(t_3 - t_2) = \frac{V_s}{L_f}(t_3 - t_2). \tag{9}$$

Because the forward voltage of a body diode is considerably small compared with V_s, $-v_f = V_s$ in (9). In this interval, $L_{\rm lk}$ is discharged, and $i_{\rm lk}$ increases from negative to zero. Moreover, $v_{\rm pri}$ decreases from positive to zero. The leakage-inductance current of the HFT can be represented as

$$i_{\rm lk}(t) = \frac{1}{n}i_{\rm pri}(t) = i_{\rm lk}(t_2) + \frac{1}{L_{\rm lk}}\int_{t_2}^{t} v_{\rm sec}(t)dt. \tag{10}$$

MODE 4 [t_3–t_4, Fig. 7(d)]: In this mode, switch S_3 is turned ON under ZVS when the deadtime ends. Because $i_{\rm pri}$ is discharged and $v_{\rm pri}$ is zero, it can be observed that L_f is charged through the same i_f path as in MODE 3.

MODE 5 [t_4–t_5, Fig. 7(e)]: When this mode begins, switches $Q_{1.2}$ and $Q_{4.2}$ are turned OFF. The leakage-inductance current of the HFT increases from zero to positive. At this point, a transient voltage ***di/dt*** on the leakage inductor of the HFT

TABLE I
PARAMETERS OF SIMULATION AND PROTOTYPE CIRCUIT

Parameter	Mark	Value	Unit
Rated power	P	±1.2	kW
Grid voltage(rms)	V_S	220	Vrms
Grid frequency	f	60	Hz
DC-link voltage	V_{dc}	400	V
Switching frequency	f_{sw}	20	kHz
Leakage inductance	L_{lk}	2.3	μH
Filter inductor	L_f	2	mH
Filter capacitor	C_f	2	μF
Turns ratio	$1{:}n$	1:1	

occurs as follows:

$$v_{\rm sec}(t) = nv_{\rm pri}(t) + L_{\rm lk}\frac{di_{\rm lk}(t)}{dt} = L_{\rm lk}\frac{di_{\rm lk}(t)}{dt}. \quad (11)$$

$v_{\rm pri}$ in (11) is zero because $i_{\rm pri}$ free wheels through S_3 and S_4. Thus, the proposed modulation scheme can eliminate the voltage spikes higher than the dc-link voltages by increasing the HFT leakage current from zero with the HFT voltage at zero.

MODE 6 [t_5–t_6, Fig. 7(f)]: At the beginning of this interval, the gate signal of S_4 changes from high to low. $v_{\rm pri}$ also decreases from zero to negative. When S_4 is completely turned OFF, $i_{\rm pri}$ flows through the body diode of S_2. This produces conditions for S_2 to be turned ON under ZVS. The secondary-side voltage reaches $-nV_{\rm dc}$, and L_f is discharged. $\Delta|i_f|$ can be expressed as

$$\Delta|i_f| = \frac{-nV_{\rm dc} + V_s}{L_f + L_{\rm lk}}(t_6 - t_5). \quad (12)$$

MODE 6 ends when S_2 begins to be turned ON, and this interval returns to MODE 1, except that $v_{\rm pri}$ and $v_{\rm sec}$ are now negative and $i_{\rm pri}$ and $i_{\rm lk}$ are now positive.

III. SIMULATION VERIFICATION

To validate the effectiveness and performance of the proposed modulation scheme for a CHFL converter, a simulation was conducted using MATLAB/Simulink. The model parameters are listed in Table I. Initially, it was confirmed that the proposed method can form the NCP in the discharging mode. Subsequently, the operational mode was converted into the charging mode by changing the power references. The performance of the proposed method is compared with those presented in [14]–[20], which did not solve the voltage-spike problems.

Fig. 8 shows an example of the gate signals generated by the proposed modulation scheme. "FB gate signals" are used for switches S_1, S_4 or S_2, S_3 of the FB converter to generate high-frequency waveforms, where ΔT represents the deadtime. The time $t_{\rm n}$ denotes the necessary time to reach the primary-side voltage of the HFT to $V_{\rm dc}$. The following equation needs to be satisfied to find the appropriate value of ΔT:

$$\frac{1}{C_{OSS}}\int_0^t i_{\rm pri}(t)dt = V_{\rm dc}. \quad (13)$$

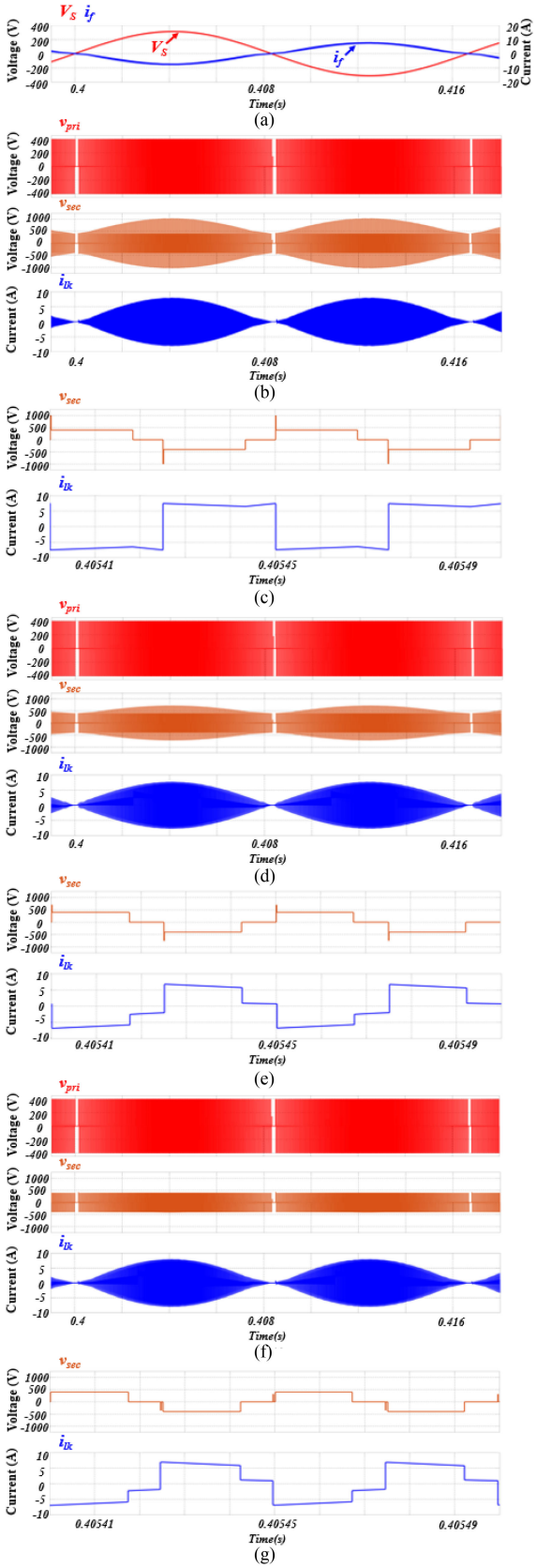

Fig. 12. (a) Simulation results of ac–dc converter in charging mode. HFT voltages and currents in the (b) and (c) primary-side modulation, (d) and (e) secondary-side modulation, and (f) and (g) proposed modulation.

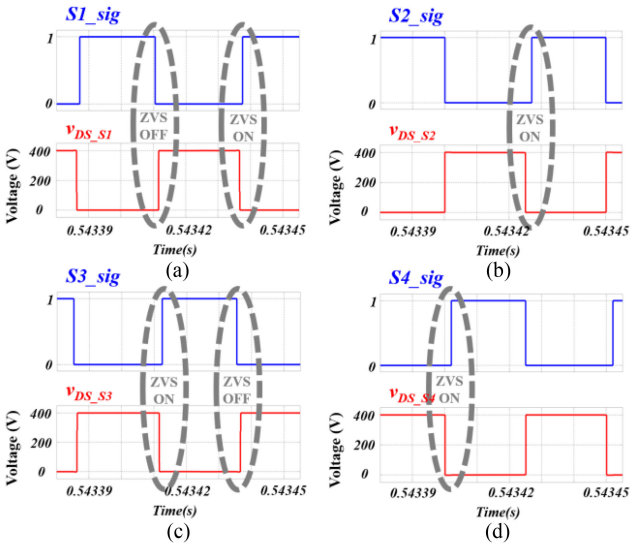

Fig. 13. Simulation results of the proposed modulation in charging mode. (a)–(d) Gate signals and drain–source voltages of FB converter.

Equation (13) can be rewritten as

$$I_{\max} \times t_n \times 0.5 \times \frac{1}{C_{OSS}} = V_{\mathrm{dc}}. \tag{14}$$

where $I_{\max}$ is the peak value of i_f. Using $I_{\max} = 7.8$ A, $V_{\mathrm{dc}} = 400$ V, and $C_{oss} = 150$ pF in (14), the time $\boldsymbol{t_n}$ in (14) can be calculated as approximately 0.02 μs. Therefore, ΔT should be greater than the sum of $\boldsymbol{t_n}$ and rising–falling time of the power switch. In this article, ΔT was selected to be 3 μs. "Cyclogate signals" represent the gate signals of the cycloconverter that operate on the basis of the deadtime of the FB gate signal. These signals are not always turned ON in the discharging mode and are employed to reduce the transient voltage ***di/dt*** in the charging mode. It can be observed, as shown in Fig. 8, that the "cyclogate signals" correspond to the gate signals of $Q_{1.2}$ and $Q_{4.2}$ if V_m is positive and the FB gate signals are the switching signals for S_1 and S_4. ΔT_1 is the deadtime to discharge the HFT leakage inductor by turning ON switch S_1 in advance before forming the free-wheeling path during the charging mode. ΔT_2 is the deadtime used for turning OFF the ac switches of the cycloconverter in the discharging mode. When the leakage inductor of the HFT is discharged, the following equation should be satisfied:

$$L_{\mathrm{lk}} \frac{-I_{\max}}{(\Delta T - \Delta T_1)} + I_{\max} R = -V_{\mathrm{dc}}. \tag{15}$$

where R is the resistance of the HFT used in this article. The resistance and leakage inductance of the HFT used in this article are 0.6 Ω and 2.3 μH, respectively. Using $I_{\max} = 7.8$ A and $V_{\mathrm{dc}} = 400$ V in (15), $(\Delta T - \Delta T_1)$ can be calculated and should be more than 0.04 μs. In this article, we set it to 0.5 μs. Since the transformer leakage inductor starts to be charged at the point where the transformer voltage is approximately 0 V, (15) can be

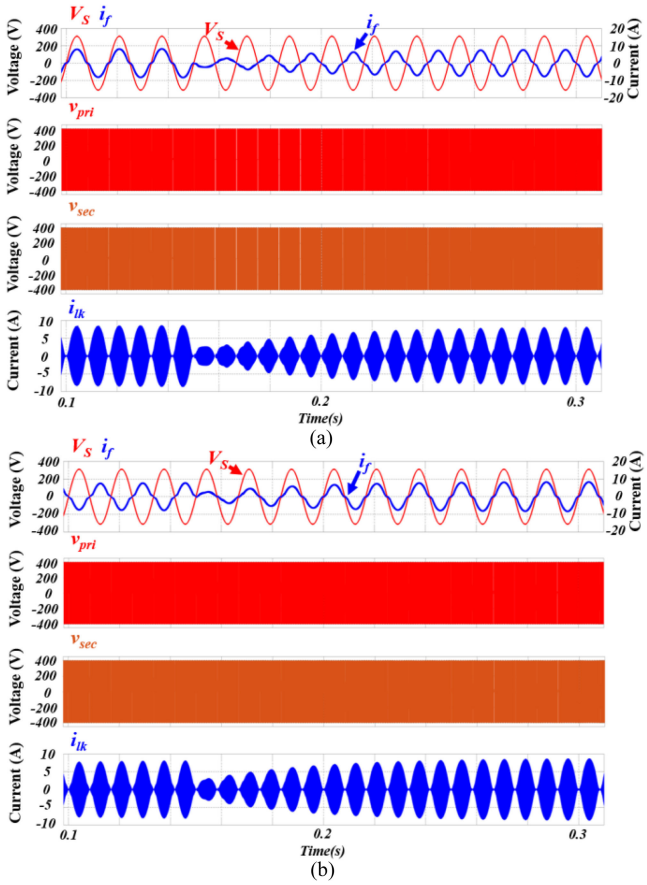

Fig. 14. Simulation results of the proposed modulation scheme during changes in operating mode. (a) From discharging to charging mode. (b) From charging to discharging mode.

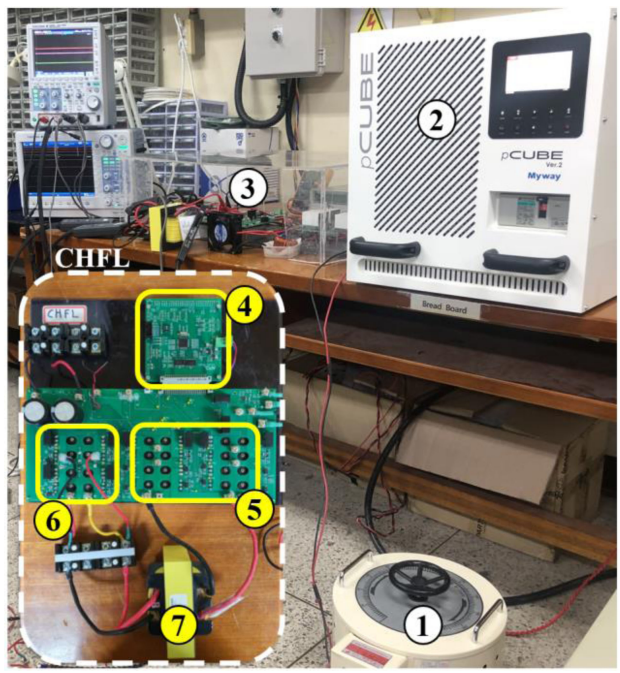

Fig. 15. Experimental test setup (1: ac power supply, 2: dc power supply, 3: ac–dc converter, 4: control board, 5: cycloconverter, 6: FB converter, 7: HFT).

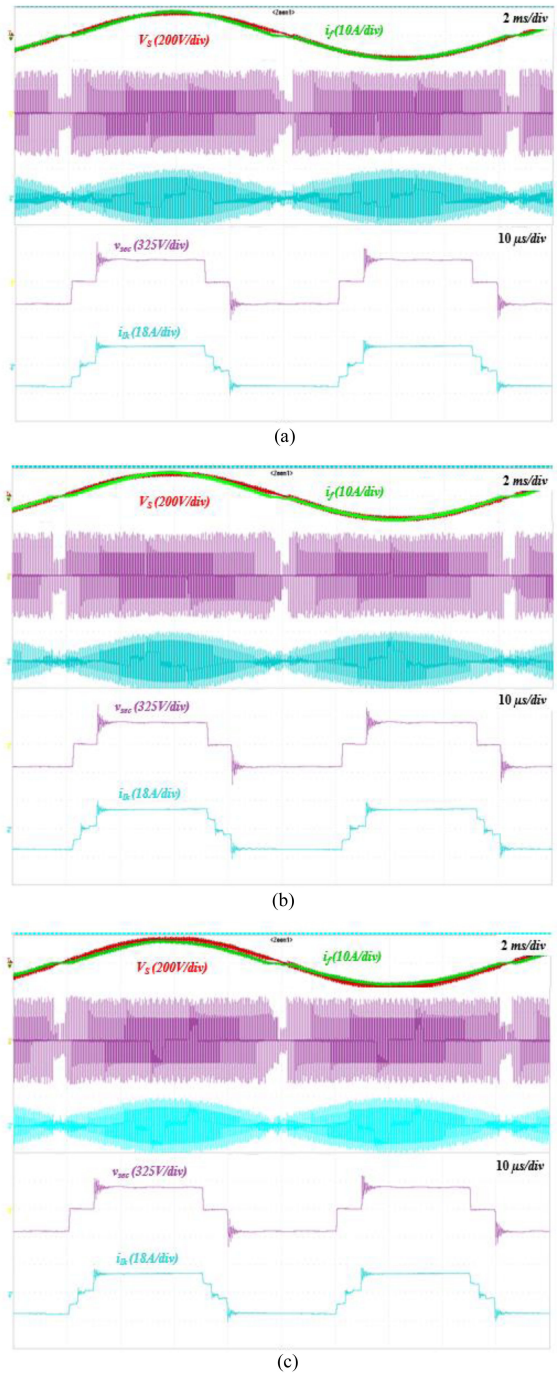

Fig. 16. Experimental results of ac–dc converter in discharging mode with dc-link voltage of 200 V and grid voltage of 110 Vrms. (a) Primary-side modulation. (b) Secondary-side modulation. (c) Proposed modulation.

rewritten as

$$L_{\rm lk}\frac{I_{\max}}{\Delta T_2}+I_{\max}R=V_{dc}. \tag{16}$$

From (16), ΔT_2 should be greater than 0.04 μs. In this article, we set it to 0.5 μs. In the primary side of the HFT, the single-phase FB converter as the dc–ac conversion system employs a phase-shift modulation method. Thus, the duty of the four power switches is 50%, and its ON-time is 25 μs, which is half of the switching period (20 kHz switching frequency) used in the study. Because a deadtime of 3 μs is used in the proposed system, the duty cycle loss is calculated as $(3/25)*100 = 12\%$. Regarding the current distortion due to the deadtime, the high-frequency voltage of the transformer in the proposed system is rectified according to the grid voltage, as shown in Fig. 9, which is the same as the line-to-line voltage of the typical single-phase FB converter using SPWM technique. Hence, the current distortion effect of the switching deadtime can be viewed the same as in a typical FB converter, resulting in odd-order harmonics in the output current [21].

Fig. 10 shows the simulation results of the proposed modulation scheme in the discharging mode. It can be observed that a natural commutation function capable of reducing or increasing $i_{\rm lk}$ smoothly, which was addressed in Section II, is achieved by the proposed method, leading to an important improvement in the HFT voltage. Fig. 11 shows the gate signals and the corresponding voltages in the FB converter and the cycloconverter. It can be confirmed that switches S_1 and S_3 in the FB are turned ON under the ZVS condition, whereas all the ac switches in the cycloconverter are turned ON/OFF under it.

Fig. 12 shows the simulation results of the proposed modulation scheme in the charging mode. The peak value of the filter inductor current is approximately equal to that in the discharging mode. However, the voltage and the current have opposite directions. The modulation methods proposed in [14]–[18] can be classified into two categories, primary- and secondary-side modulations. In the former category [14]–[16], the FB converter regulates the amount of the delivered power, whereas in the latter methods [17]–[18], the cycloconverter controls the power.

Fig. 12(b) and (c) depicts the HFT voltage and current waveforms in the primary-side modulation. A maximum voltage spike of approximately 1000 V on the HFT secondary side is observed because of the significant change in the HFT leakage current from negative to positive or from positive to negative. It can be observed from Fig. 12(d) and (e) that the secondary-side modulation has a smaller voltage spike of approximately 750 V than that in the primary-side modulation. This is because the FB converter discharges the HFT leakage current before the free-wheeling path is formed and subsequently recharges it. It is worth mentioning that the magnitude of the voltage spike is still greater than the dc-link voltage; therefore, a better modulation method is required to improve system reliability. Fig. 12(f) and (g) depicts the simulation results of the proposed modulation scheme. It is evident that the voltage spike in the HFT secondary side is significantly eliminated, as expected. Because the proposed method can discharge the leakage current similarly with the secondary-side modulation method and, subsequently, recharging it in advance under zero HFT voltage during MODE 5, as depicted in Fig. 7(e).

Fig. 13 presents the gating signals and drain–source voltages of the FB converter obtained from the simulations. It can be observed that the switches S_1 and S_3 are turned ON/OFF under the ZVS condition, whereas all remaining switches of the FB converter are turned ON under the ZVS condition.

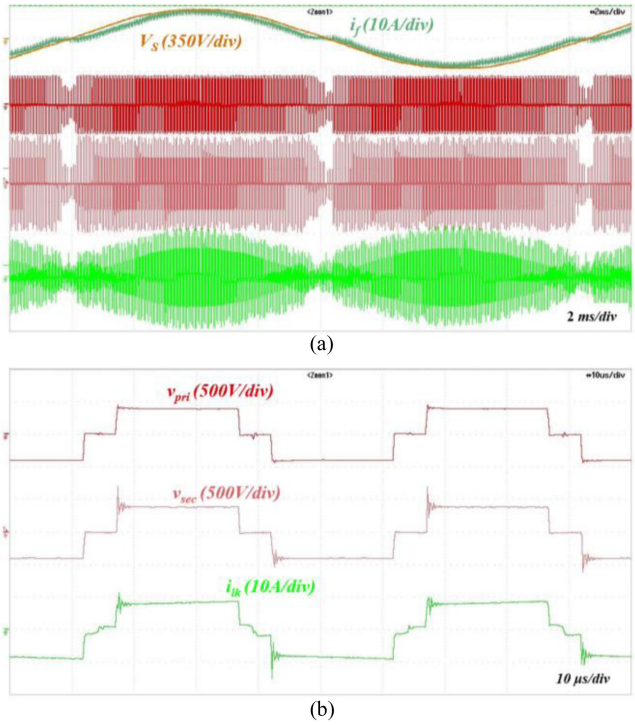

Fig. 17. Experimental results. (a) Voltages and current in discharging mode. (b) Magnified experimental waveforms in discharging mode.

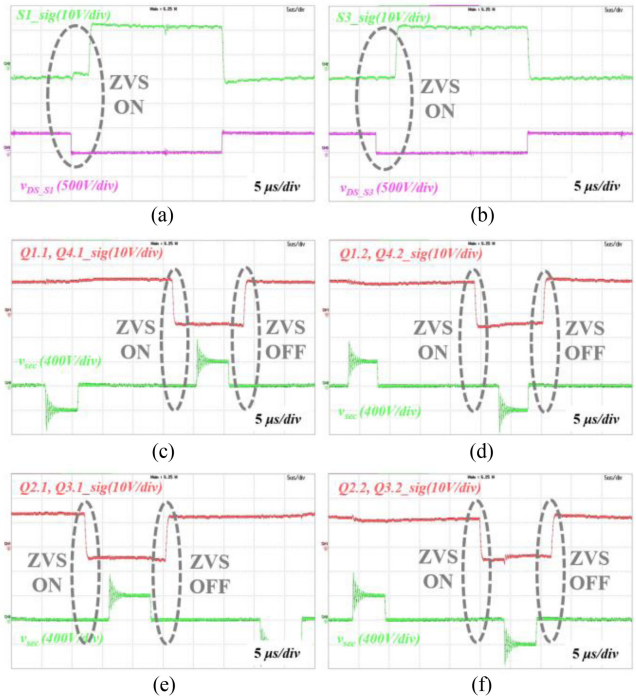

Fig. 18. Experimental results of the proposed modulation in discharging mode. (a) and (b) Gate signals and drain–source voltages of FB converter. (c)–(f) Gate signals and input voltage of cycloconverter.

Fig. 14 shows the transient waveforms under a rapid power flow change from charging to discharging mode or vice versa. It can be observed from the results that the seamless mode transfer can be achieved without high-voltage spikes in the bidirectional ac–dc converter using the proposed modulation scheme.

IV. Experimental Verification

A 1.2-kW prototype CHFL converter was built to evaluate the performance of the proposed modulation scheme. The parameters of the prototype system are the same as the simulation parameters listed in Table I. Fig. 15 shows the experimental test setup and the prototype board of the CHFL converter connected to the grid. The silicon-carbide metal–oxide–semiconductor field-effect transistor (MOSFET) used in both the FB converter and cycloconverter is C2M0040120D manufactured by CREE, and these power devices are driven by the gate driver IC ACPL-W346 manufactured by Broadcom. The control algorithms, including the proposed modulation scheme, are realized using the digital controller TMS320F28069 manufactured by Texas Instruments. The experimental tests were performed in the same order as the simulations. However, it is worth addressing that in the comparative experiment the test conditions of the input ac voltage and dc voltage were modified as 110 Vac and 200 Vdc, respectively. Because the high-voltages spikes resulting from the conventional modulation schemes exceed the maximum voltage allowed by the HFT and the breaking voltage of the power devices and, thus, may damage these components.

Fig. 16 shows the experimental results of the HFT secondary-side voltage in the discharging mode to evaluate the performance of the proposed method in suppressing the voltage spikes compared with the two conventional methods reported in [14]–[18]. It can be observed that all the three methods demonstrate similar levels of performance in suppressing the voltage spike in the discharging mode.

Fig. 17 presents the experimental results in the discharging mode during the steady state. As shown in the simulation results, the proposed modulation scheme can provide a natural commutation function capable of reducing or increasing i_{lk} naturally. Fig. 18 shows the corresponding switching signals and switch voltages verifying the ZVS operation. It can be noted that switches S_1 and S_3 in the FB converter are turned ON under the ZVS condition, whereas all ac switches in the cycloconverter are turned ON/OFF under it, as discussed in Section II.

Fig. 19 shows the experimental results of the HFT secondary-side voltage in the charging mode. Compared with Fig. 16, the experimental results corresponding to the voltage spike are significantly distinguishable. It can be observed that the primary-side modulation leads to the highest voltage spike of approximately 700 V even under the 200 Vdc condition. This is followed by that in the secondary-side modulation of approximately 500 V. In contrast, under the proposed modulation scheme, the voltage spike is approximately 400 Vdc, showing that it can reduce the voltage spike the most among the three modulation schemes, because the HFT leakage current can be charged under the zero HFT voltage.

Fig. 20 shows the experimental results of the key waveforms in the charging mode during the steady state. It can be observed that the peak filter inductor current is approximately equal to that in the discharging mode, except that the direction of the

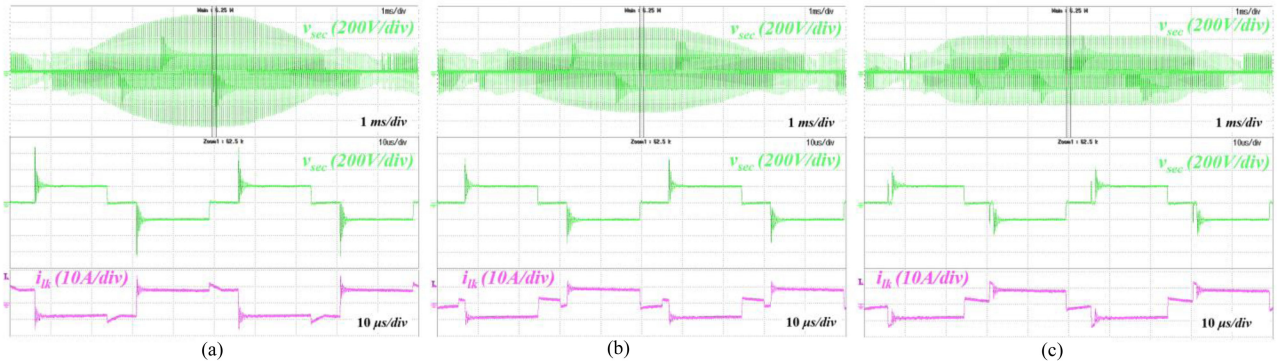

Fig. 19. Experimental results of ac–dc converter in charging mode with dc-link voltage of 200 V and grid voltage of 110 Vrms. (a) Primary-side modulation. (b) Secondary-side modulation. (c) Proposed modulation.

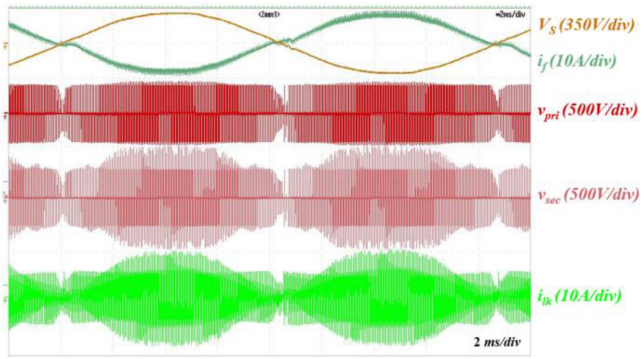

Fig. 20. Experimental results of ac–dc converter in charging mode.

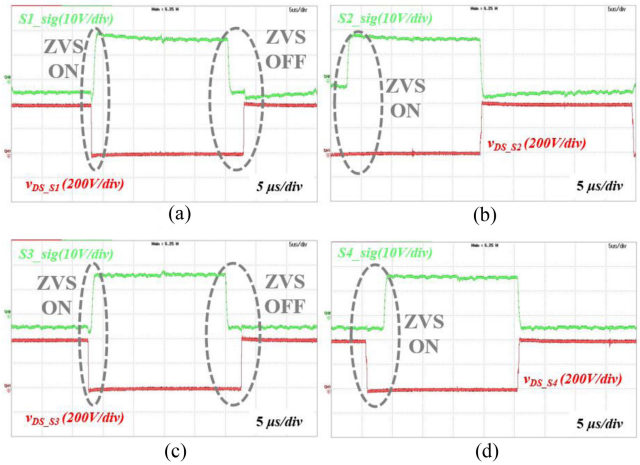

Fig. 21. Experimental results of the proposed modulation in charging mode. (a)–(d) Gate signals and drain–source voltages of FB converter.

voltage and current is different. Fig. 21 shows the corresponding switching signals and switch voltages. It can be observed in the experimental results corresponding to the discharging mode, ZVS operation can be achieved in the charging mode by the proposed modulation scheme. It is worth mentioning that the ringing voltage (V_{ringing}) on the HFT secondary side during both the operation modes is caused by the leakage inductance of the transformer and the parasitic capacitance of the MOSFET.

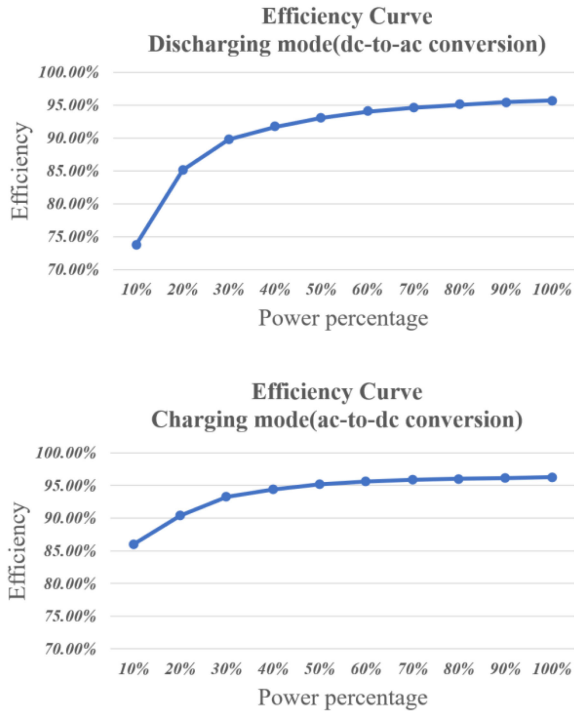

Fig. 22. Experimentally measured efficiency of the bidirectional ac–dc converter prototype.

The frequency (f_{ringing}) of the ringing voltage can be determined from the following equations [22]:

$$V_{\text{ringing}} = V_{\text{dc}} \cdot n \cdot (1 + 80\%). \tag{17}$$

$$f_{\text{ringing}} = \frac{1}{2\pi\sqrt{n^2 L_{\text{lk}} C_{OSS}}}. \tag{18}$$

Additionally, experimentally measured efficiency of the bidirectional ac–dc converter employing the proposed modulation scheme at both operating modes is shown in Fig. 22. These data were measured using HIOKI PW3390 power analyzer.

V. Conclusion

For high-power density and long-life converters, ac–ac the power conversion structure that does not require any intermediate filter components is a good candidate; however, the switching signals should be generated carefully owing to the usage of bidirectional power devices. In this article, we proposed an improved modulation scheme to reduce the high-voltage spikes in both discharge and charge power flow directions for isolated bidirectional ac–dc converters. The performance of the proposed method was verified with simulation studies and on an experimental system. In fact, compared with two conventional modulation schemes, the proposed method has reduced the voltage-spike magnitude by more than 50% while providing simple switching-signal generation. Additionally, the proposed method enables ZVS operation in both operation modes. Thus, the proposed modulation scheme is capable of improving the reliability and efficiency of the converter system for various bidirectional power flow applications.

References

[1] R. Morrison and M. G. Egan, "A new power-factor-corrected single-transformer UPS design," *IEEE Trans. Ind. Appl.*, vol. 36, no. 1, pp. 171–179, Jan./Feb. 2000.

[2] S. K. Mazumder, R. K. Burra, R. Huang, M. Tahir, and K. Acharya, "A universal grid-connected fuel-cell inverter for residential application," *IEEE Trans. Ind. Electron.*, vol. 57, no. 10, pp. 3431–3447, Oct. 2010.

[3] M. Yilmaz and P. T. Krein, "Review of battery charger topologies, charging power levels, and infrastructure for plug-in electric and hybrid vehicles," *IEEE Trans. Power Electron.*, vol. 28, no. 5, pp. 2151–2169, May 2013.

[4] S. B. Kjaer, J. K. Pedersen, and F. Blaabjerg, "A review of single-phase grid-connected inverters for photovoltaic modules," *IEEE Trans. Ind. Appl.*, vol. 41, no. 5, pp. 1292–1306, Sep./Oct. 2005.

[5] K. V. Iyer, R. Baranwal, and N. Mohan, "A high-frequency ac-link single-stage asymmetrical multilevel converter for grid integration of renewable energy systems," *IEEE Trans. Power Electron.*, vol. 32, no. 7, pp. 5087–5108, Jul. 2017.

[6] G. E. Sfakianakis, J. Everts, and E. A. Lomonova, "Overview of the requirements and implementations of bidirectional isolated ac-dc converters for automotive battery charging applications," in *Proc. 10th Int. Conf. Ecol. Veh. Renewable Energies*, Monte Carlo, Monaco, 2015, pp. 1–12.

[7] F. Krismer and J. W. Kolar, "Efficiency-optimized high-current dual active bridge converter for automotive applications," *IEEE Trans. Ind. Electron.*, vol. 59, no. 7, pp. 2745–2760, Jul. 2012.

[8] O. C. da Silva Filho, B. R. de Almeida, D. de Souza Oliveira, and T. R. F. Neto, "High-frequency isolated ac–dc–ac interleaved converter for power quality applications," *IEEE Trans. Ind. Appl.*, vol. 54, no. 5, pp. 4594–4602, Sep./Oct. 2018.

[9] D. Chen and Y. Chen, "Step-up ac voltage regulators with high-frequency link," *IEEE Trans. Power Electron.*, vol. 28, no. 1, pp. 390–397, Jan. 2013.

[10] J. Mahlein, M. Bruckmann, and M. Braun, "Passive protection strategy for a drive system with a matrix converter and an induction machine," *IEEE Trans. Ind. Electron.*, vol. 49, no. 2, pp. 297–303, Apr. 2002.

[11] W. Zhu, K. Zhou, M. Cheng, and F. Peng, "A high-frequency-link single-phase PWM rectifier," *IEEE Trans. Ind. Electron.*, vol. 62, no. 1, pp. 289–298, Jan. 2015.

[12] N. Kummari, S. Chakraborty, and S. Chattopadhyay, "Secondary side modulation of a single-stage isolated high-frequency link microinverter with a regenerative flyback snubber," in *Proc. IEEE Energy Convers. Congr. Expo.*, Milwaukee, WI, USA, 2016, pp. 1–8.

[13] X. Zhou, J. Xu, and S. Zhong, "Single-stage soft-switching low-distortion bipolar PWM modulation high-frequency-link dc–ac converter with clamping circuits," *IEEE Trans. Ind. Electron.*, vol. 65, no. 10, pp. 7719–7729, Oct. 2018.

[14] Z. Yan, S. Xu, X. Han, X. Guo, and C. Zhang, "A waveform control strategy for single-phase high-frequency link matrix inverter," in *Proc. 40th Annu. Conf. IEEE Ind. Electron. Soc.*, Dallas, TX, USA, 2014, pp. 4834–4839.

[15] R. K. Surapaneni, D. B. Yelaverthi, and A. K. Rathore, "Cycloconverter-based double-ended microinverter topologies for solar photovoltaic ac module," *IEEE J. Emerg. Sel. Topics Power Electron.*, vol. 4, no. 4, pp. 1354–1361, Dec. 2016.

[16] S. Norrga, "Experimental study of a soft-switched isolated bidirectional ac–dc converter without auxiliary circuit," *IEEE Trans. Power Electron.*, vol. 21, no. 6, pp. 1580–1587, Nov. 2006.

[17] M. Wang, S. Guo, Q. Huang, W. Yu, and A. Q. Huang, "An isolated bidirectional single-stage dc–ac converter using wide-band-gap devices with a novel carrier-based unipolar modulation technique under synchronous rectification," *IEEE Trans. Power Electron.*, vol. 32, no. 3, pp. 1832–1843, Mar. 2017.

[18] M. Wang, Q. Huang, S. Guo, X. Yu, W. Yu, and A. Q. Huang, "Soft-switched modulation techniques for an isolated bidirectional dc–ac," *IEEE Trans. Power Electron.*, vol. 33, no. 1, pp. 137–150, Jan. 2018.

[19] S. Guo, X. Ni, K. Tan, and A. Q. Huang, "Operation principles of bidirectional isolated ac/dc converter with natural clamping soft switching scheme," in *Proc. 40th Annu. Conf. IEEE Ind. Electron. Soc.*, Dallas, TX, USA, 2014, pp. 4866–4872.

[20] F. Wu, X. Li, and S. Luo, "Improved modulation strategy for single-phase single-stage isolated ac–dc converter considering power reversion zone," *IEEE Trans. Power Electron.*, vol. 35, no. 4, pp. 4157–4167, Apr. 2020.

[21] U.-S. Seong, J.-S. Lee, S.-H. Hwang, and J.-M. Kim, "Dead time compensation of single-phase grid-connected inverter using SOGI," *Trans. Korean Inst. Power Electron.*, vol. 22, no. 2, pp. 166–174, 2017.

[22] J. A. Sabate, V. Vlatkovic, R. B. Ridley, F. C. Lee, and B. H. Cho, "Design considerations for high-voltage high-power full-bridge zero-voltage-switched PWM converter," in *Proc. 5th Annu. Proc. Appl. Power Electron. Conf. Expo.*, Los Angeles, CA, USA, 1990, pp. 275–284.

Jeong-Tae Kim (Student Member, IEEE) received the B.S. and M.S. degrees in electronics and electrical engineering from Hongik University, Sejong, South Korea, in 2020 and 2022, respectively.

He is currently with Hyundai Mobis, Yongin, South Korea. His research interests include power electronics' applications for electric vehicles and renewable energy systems.

Sung-Min Park (Member, IEEE) received the B.S. degree in electronics engineering and the M.S. degree in electrical engineering from Korea University, Seoul, South Korea, in 2001 and 2003, respectively, and the Ph.D. degree from the Department of Electrical and Computer Engineering, University of Connecticut, Storrs, CT, USA, in 2015.

From 2003 to 2008, he was a Senior Engineer with LG Electronics, Seoul, South Korea. From 2008 to 2010, he was with Samsung Heavy Industries, Suwon, South Korea. From 2014 to 2015, he was a Senior Research Engineer with United Technologies Research Center, East Hartford, CT, USA. He is currently an Associate Professor with the Department of Electronic and Electrical Engineering, Hongik University, Sejong, South Korea. His research interests include power electronics' applications for electric vehicles, home appliances, and renewable energy systems.